Thermodynamics of excitonic molecules in silicon

P. L. Gourley and J. P. Wolfe
Physics Department and Materials Research Laboratory,
University of Illinois at Urbana-Champaign, Urbana, Illinois 61801
(Received 30 November 1978)

The first spatially controlled thermodynamic measurements of a system of free excitons (FE) and excitonic molecules (EM) are reported. Both excitonic phases are confined to Gaussian spatial distributions in a strain-induced potential well. This parabolic well affords a simple analytic description of the thermal expansion of the gases. Recombination emission from the ultrapure Si is detected with spatial, spectral, and time resolution over the temperature range 3.5–10 K. The system is well described by a chemical equilibrium between two ideal gases at the lattice temperature: we observe the quadratic dependence of the EM density on the FE density and the expected form of thermal activation. In addition, the EM-FE thermalization time is found to be much less than the recombination times. The thermodynamically determined binding energy, $\phi_{EM}^{t} = 1.53 \pm 0.10$ meV, is in excellent agreement with our measured spectroscopic value $\phi_{EM}^{s} = 1.46 \pm 0.09$ meV. These values are several times larger than the most recent theoretical estimates.

I. INTRODUCTION

The possibility that two excitons in a semiconductor can bind to form a molecular complex was initially proposed by Lampert.[1] The search for excitonic molecules (EM) has evoked considerable interest and controversy. Both experimental and theoretical evidence for EM in the direct-gap materials have been reported.[2] In the indirect-gap semiconductors Si and Ge, luminescence lines originally attributed to EM are now generally interpreted as emission from the electron-hole liquid (EHL) phase. Indeed, the multivalley electronic band structure of elemental semiconductors permits a highly stable liquid phase which almost precludes the formation of EM in detectable numbers. On the other hand, the short recombination times in direct-gap materials prevent a complete thermalization of the excitonic phases by the crystal lattice. A spectroscopic observation of EM in the indirect-gap semiconductor AgBr was reported by Pelant *et al.*,[3] but likewise the short EM decay time (20 ns) prevented thermal equilibrium with the lattice.

New spectroscopic evidence for the existence of EM in Si has recently emerged. By applying uniform stress to reduce the valley degeneracy and consequently the EHL binding energy, Kulakovskii and Timofeev[4,5] have observed a new luminescence peak with energy position intermediate to the free exciton (FE) and EHL. The reported decay time was about 0.2 μs. Also, the present authors observed a similar peak (same spectral position but narrower width) accompanying the emission from EHL and FE coexisting in a strain-induced potential well.[6] Decay times of these photoexcited phases exceeded 2 μs. Figure 1 shows the TA-phonon-assisted replica of this luminescence at an excitation level below the EHL threshold. The low-energy emission peak is attributed to a radiative recombination of one of the two electron-hole pairs of the excitonic molecule, leaving a single exciton after the decay. Independently, Thewalt and Rostworski[7] have observed for the first time a similar, though weaker, EM emission line in *unstressed* Si. No comparable data exist for Ge, where the excitonic Rydberg is 5× smaller than in Si, although Thomas and Rice[8] have suggested that molecules may be partly responsible for a broadening of the FE line in Ge.

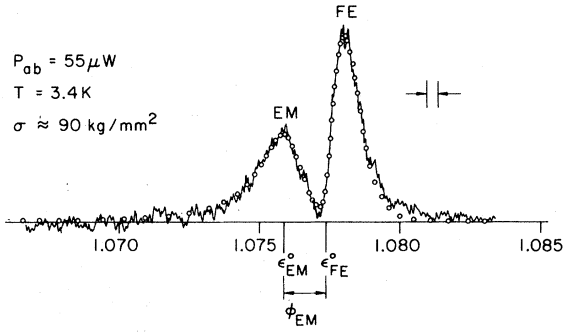

FIG. 1. TA replica of the luminescence at low absorbed laser power and composite least-squares fit (open points). Here $\epsilon_{EM}^{0} = E_{EM} - \hbar\omega_{TA} - E_{FE}$ and $\epsilon_{FE}^{0} = E_{FE} - \hbar\omega_{TA}$ where $\hbar\omega_{TA}$ is the TA-phonon energy. This luminescence from the highly stressed, ultrapure Si crystal was detected by photon counting. All other cw data reported here examine the TO-LO replica using the experimental methods described in Ref. 6. Stress $\equiv \sigma$.

This paper provides strong thermodynamic support for the existence of the EM in Si based on spatial, spectral, and time-resolved measurements of the recombination luminescence. With steady-state excitation the EM-FE system is well described by a local chemical equilibrium as evidenced by a near-quadratic relation between the EM and FE densities and the expected Arrhenius form of thermal activation. The time-decay measurements are consistent with the steady-state observations indicating that the EM-FE thermalization times are much shorter than the recombination lifetimes.

II. SPATIAL DISTRIBUTION AND LOCAL EQUILIBRIUM

The EM-FE equilibrium was achieved by confining the excitonic gas to a Gaussian distribution in a parabolic strain potential well which was created about 0.3 mm inside the Si crystal with a Hertzian stress geometry.[6,9] This was accomplished by stressing the crystal along a ⟨100⟩ axis with a rounded stainless-steel plunger and by optically exciting with an Ar^+ (surface excitation) or YAlG : Nd (volume excitation) laser. A vidicon image of the resulting photoluminescence at $T \approx 10$ K with surface excitation at the left crystal face is shown in Fig. 2. The parabolic strain well affords both spatial confinement and reduced EHL binding energy, allowing the high FE concentrations necessary to form EM in appreciable numbers even with low-level, steady-state excitation.

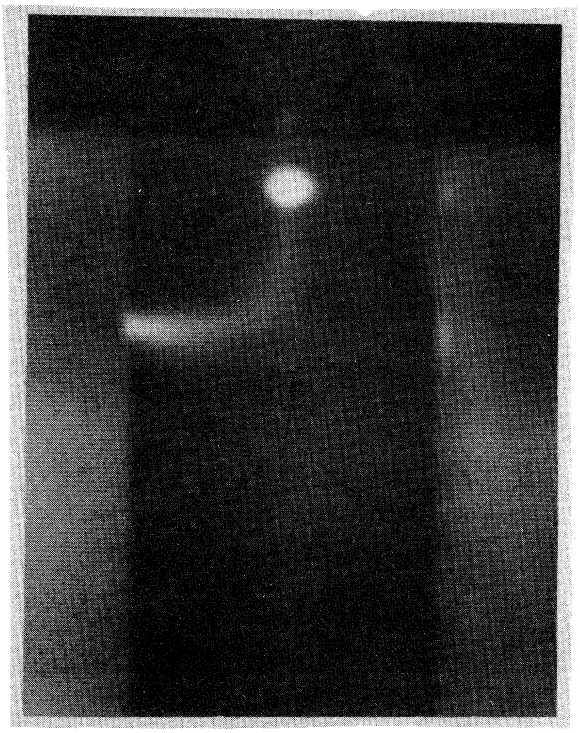

FIG. 2. Exciton luminescence emanating from a $1.5 \times 1.5 \times 4$ mm^3 crystal of ultrapure Si at $T \approx 10$ K. The top crystal surface, accurately flattened and polished, is pressed with a spherical contacting surface of a steel plunger cut from a ball bearing with radius $R = 3.8$ cm. Excitons produced at the left crystal surface by a cw Ar laser are drawn into a parabolic potential well corresponding to a shear strain maximum beneath the plunger.

This stress geometry enabled a simple analytic description of the EM and FE spatial distributions. The equilibrium distribution of particles in a three-dimensional parabolic potential well $V_i(r) = \alpha_i r^2$ may be determined by requiring spatial invariance of the chemical potential.[10] The result is that the local particle density is given by

$$n_i(r) = n_i(0) \exp(-\alpha_i r^2/kT) , \quad (1)$$

where the subscript i refers to the type of particle (EM or FE) and $n_i(0) = (\alpha_i/\pi kT)^{3/2} N_i$ where N_i is the total number of particles in the gas which has effective volume $V_i = (\pi kT/\alpha_i)^{3/2}$. The full width at half maximum (FWHM) of this distribution is $\Delta_i = (2.77kT/\alpha_i)^{1/2}$.[11] This last result also follows from the equipartition theorem and states that the mean-square particle displacement is determined solely by temperature and the restoring force constant α. Thus under equilibrium conditions neither the density of particles nor their lifetimes will affect the spatial distribution of the gas. This result forms the basis for our thermodynamic measurements.

The above ideas have been experimentally verified: the spatial extent of the confined excitonic gas expands as $T^{1/2}$ and is independent of excitation level,[6] whereas the central density at a given temperature is controlled directly by the excitation level. Since the EM consists of two electron hole (e-h) pairs while FE is a single e-h pair, we expect that $\alpha_{EM} = 2\alpha_{FE}$, implying that $\Delta_{EM} = 0.75\Delta_{FE}$.

The measured spatial profiles of the EM and FE distributions are shown in Fig. 3. Indeed, the EM distribution is narrower than that of the FE. A Gaussian function (solid points) provides an excel-

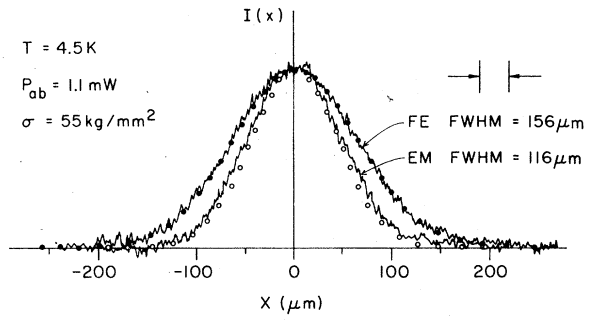

FIG. 3. Spatial profiles of the EM and FE distributions obtained by scanning the image of the crystal across the entrance slit of a monochromator set at the respective wave length.

lent fit to the FE profile. The square of this function (open points) very nearly fits the EM profile, showing that the system is close to a local chemical equilibrium. An excellent fit to the EM profile is obtained with a Gaussian function with $\Delta_{EM}=0.75\Delta_{FE}$ (not plotted).

III. CHEMICAL EQUILIBRIUM

The single-particle partition functions for EM and FE with energies parabolic in all phase-space coordinates (cf. discussion in the Appendix) are given by

$$\zeta_i = \frac{g_i}{(2\pi)^3}\int d^3k \int d^3r \times \exp\left[-\left(\frac{\hbar^2k^2}{2m_i}+\alpha_i r^2+E_i\right)\Big/kT\right]$$

$$= g_i\left(\frac{m_i kT}{2\pi\hbar^2}\right)^{3/2}\left(\frac{\pi kT}{\alpha_i}\right)^{3/2} e^{-E_i/kT}, \tag{2}$$

where we consider only the ground-state energies, E_i, and m_i are effective masses, g_i are degeneracy factors, and $2E_{FE}-E_{EM}=\phi_{EM}$ is the molecular binding energy. The condition for chemical equilibrium is

$$\frac{\zeta_{FE}^2}{\zeta_{EM}} = \frac{N_{FE}^2}{N_{EM}} \equiv N^*(T), \tag{3a}$$

with

$$N^*(T) = \frac{g_{FE}^2}{g_{EM}}\left(\frac{1}{2\hbar^2}\frac{m_{FE}^2}{m_{EM}}\frac{\alpha_{EM}}{\alpha_{FE}^2}\right)^{3/2}(kT)^3 \times \exp(-\phi_{EM}/kT). \tag{3b}$$

The equilibrium constant $N^*(T)$ is independent of the total number of e-h pairs in the well and therefore independent of the excitation level and the e-h pair collection efficiency of the strain well. The temperature dependence differs from the free-particle form, $T^{3/2}\exp(-\phi_{EM}/kT)$, by a factor $T^{3/2}$ due to thermal expansion of the effective volume. Thus expansions of the spatial distributions are incorporated directly into the equation for chemical equilibrium. In uniformly stressed or unstressed crystals, the temperature dependence of the particle distribution is more complicated since it depends on diffusion and excitation geometry. For a spatial distribution controlled by diffusion, the effective volume depends on the diffusion constant and the lifetime, both of which can be temperature dependent. In Si the FE lifetimes are strongly temperature dependent (cf. Sec. V and Ref. 14).

We emphasize that the knowledge of the temperature dependence of the spatial distributions is an essential part of the thermodynamic determination of the binding energy. Failure to account for an expanding V_i with temperature would result in an artificially small value for ϕ_{EM}^L.

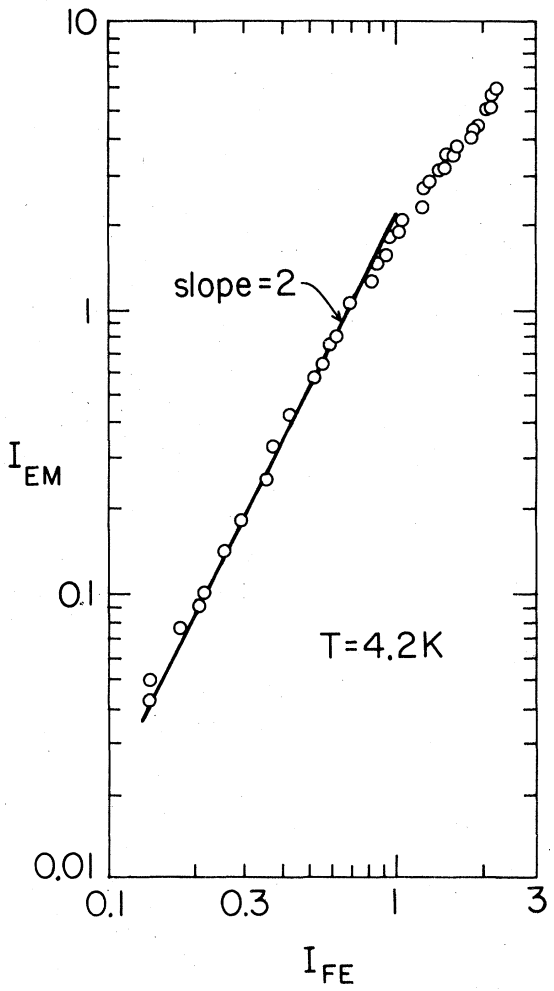

FIG. 4. Dependence of the EM peak height (I_{EM}) on the FE peak height (I_{FE}) as the excitation level is increased.

The fundamental relation of chemical equilibrium, the square law of Eq. (3a), is experimentally verified by the power dependence of Fig. 4. The EM emission line has a peak height which increases quadratically with the FE peak height, as predicted by Eq. (3a), and maintains a constant spectral shape. At higher excitation levels the departure from the slope of 2 coincides with the appearance of the EHL peak in the low-energy tail of the EM line. The excitation level for all other data reported in this paper was restricted to the low-power region where the "square-law" holds. Figure 4 also demonstrates the absence of crystal heating at these low-excitation levels.

A temperature dependence of the luminescence collected from the entire well is shown in Fig. 5. The temperature broadening of both line shapes is caused

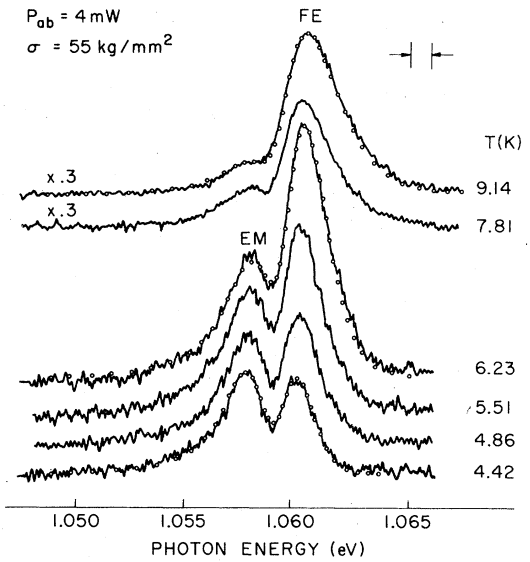

FIG. 5. Temperature dependence of the TO-LO replica of the luminescence showing the dissociation of EM to FE with increasing temperature.

by thermal expansion of the gas into higher energy regions of the strain well. The rapid increase of the ratio of FE to EM integrated intensities demonstrates the sharp temperature dependence of $N^*(T)$ in Eq. (3b). The EM line shape exhibits a long, low-energy tail that is independent of temperature. This tail corresponds to the distribution of kinetic energies for the FE remaining after the radiative EM decay.

IV. MOLECULAR BINDING ENERGY

The fact that the emission lines and their overlap changed with temperature necessitated a spectral analysis to isolate the EM and FE line shapes in order to determine the relative number of particles. The measured spectra were fit by least squares to a superposition of Cho's EM line shape[12] and a Gaussian-broadened FE line. Both line shapes include an initial density of states $D(\epsilon) \sim \epsilon^2$ appropriate for the parabolic well.[6] The line-shape functions employed the measured lattice temperature and the superposition was convolved with the measured spectrometer slit function. A detailed description of the fitting procedure is presented in the Appendix. Figure 5 includes least-square fits (open points) at low, intermediate, and high temperature showing that the spectra are well described by the measured lattice temperature. Below about 6 K where the peaks are well resolved, the fitting parameters [energy positions (2), broadening parameters (2), and relative height

TABLE I. Average values of spectroscopic fitting parameters (in meV).

Stress geometry	Phonon replica	N^c	ϵ_0	σ_G	ϕ_{EM}^{ℓ}
PW[a]	TO-LO	18	1.15 ± 0.15	0.16 ± 0.10	1.45 ± 0.09
PW[a]	TA	4	0.90 ± 0.10	0.11 ± 0.05	1.47 ± 0.08
U[b]	TO-LO	3	1.19 ± 0.07	0.28 ± 0.04	1.40 ± 0.03

[a]PW: Potential well. [c]N: Number of spectra.
[b]U: Uniform.

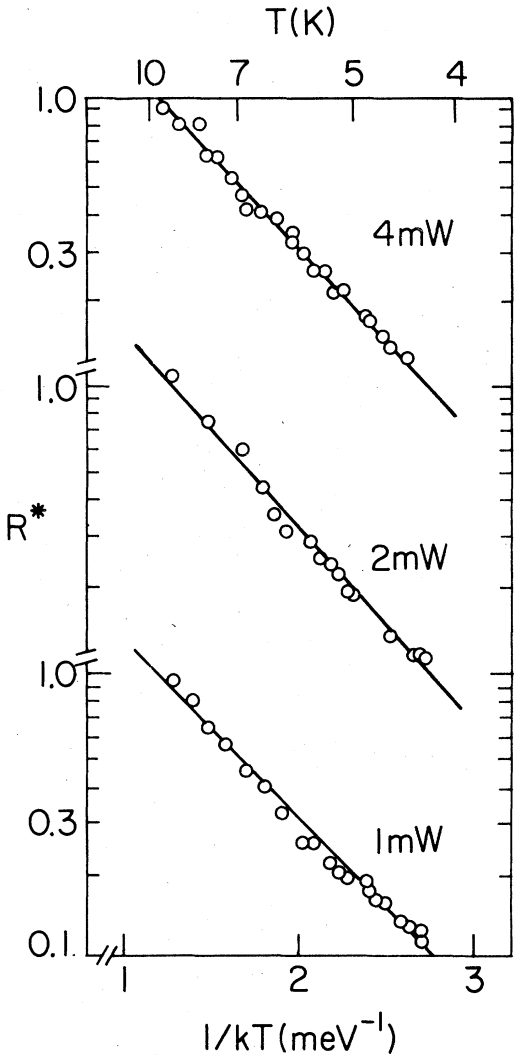

FIG. 6. Thermodynamic determinations of the binding energy at three different excitation levels. Here $R^*(T) = N_{FE}^2/N_{FE}\,T^3$. The solid lines are least-squares fits to the data points which yield $\phi_{EM}^{\ell} = 1.43$, 1.56, and 1.50 meV for the 1, 2, and 4 mW data, respectively. These plots actually lie on top of each other as a consequence of the power independence of R^*.

(1)] were quite independent of each other. Figure 1 is a fit to the TA replica of the luminescence at 3.4 K, where the EM and FE lines are almost completely separated. Both TA and TO-LO replicas were fit with a single replica of the fitting function described in the Appendix. Fits to both replicas give nearly identical binding energies, although the EM-FE linewidths were slightly broader in the TO-LO replica. The mean spectroscopic binding energy for 22 spectra with various temperatures, stresses, and phonon replicas was $\phi_{EM}^{s} = 1.46 \pm 0.09$ meV. The average values of the spectroscopic fitting parameters for each replica are summarized in Table I.

The relative values of N_{EM} and N_{FE} were calculated for each temperature by numerical integration of the isolated EM and FE line shapes. As seen from Eqs. (3), a semilog plot of the ratio $R^* \equiv N^*/T^3$ versus reciprocal temperature provides a thermodynamic determination of ϕ_{EM}. In Fig. 6 three such plots at different excitation level demonstrate, within the accuracy of the experiment, that the activation energy is independent of the density of particles in the strain well. Six different T dependences at different excitation level and stress yielded a thermodynamic binding energy $\phi_{EM}^{t} = 1.53 \pm 0.10$ meV.

Kulakovskii and Timofeev,[13] have reported a thermal activation energy of 0.55 meV under different experimental conditions. They observed the EM and FE intensities from $T = 1.8$–4.2 K in a uniformly stressed sample. Since the temperature dependence of the spatial distributions was not measured in their experiments the exact temperature dependence of the pre-exponential factor in the equilibrium constant is uncertain. This prevents a direct comparison with their data at this time.

V. CHEMICAL KINETICS

An essential condition for the existence of chemical equilibrium between FE and EM is that the intersystem thermalization times be short compared to the particle lifetimes. This condition is not easily met for direct-gap semiconductors with nanosecond recombination times. For excitonic particles in Si, however, it is possible to demonstrate that the particle lifetimes are much longer than this, permitting thermalization of photoexcited pairs to occur.

We have investigated a set of local kinetic equations for an excitonic system similar to that described by Hammond and Silver[14] but extended to include EM and saturation effects. The equations include finite lifetimes, capture and evaporation at impurities, and formation and dissociation of EM. The salient features of the EM-FE equilibrium relevant to this discussion are most easily seen at low temperature, and at densities below the saturation of impurity levels. With these simplifications it is possible to reduce this more complete set of rate equations to the pair of coupled differential equations for EM and FE.[15–18]

$$\frac{dn_{FE}}{dt} = J - \frac{n_{FE}}{\tau_{FE}} + \frac{n_{EM}}{\tau_{EM}} - 2bn_{FE}^2 + 2bn^* n_{EM} , \quad (4a)$$

$$\frac{dn_{EM}}{dt} = -\frac{n_{EM}}{\tau_{EM}} + bn_{FE}^2 - bn^* n_{EM} . \quad (4b)$$

Here J is the generation rate of FE assuming very fast thermalization of free carriers into FE, $n^* = N^*/V^*$ with $V^* = V_{FE}^2/V_{EM}$, and $b = \sigma v$, where σ is the total cross section involved in molecule formation from exciton-exciton collisions and v is the FE thermal velocity. Capture of FE and EM at impurities is included in the total recombination lifetimes τ_i.

The steady-state densities, n_i^0, are

$$n_{EM}^0 = \frac{b(n_{FE}^0)^2}{\tau_{EM}^{-1} + bn^*} , \quad (5a)$$

$$n_{FE}^0 = n^* \frac{\tau_{EM}}{2\tau_{FE}} \left(1 + \frac{1}{bn^* \tau_{EM}}\right) \times [-1 + (1 + J/J_0)^{1/2}] , \quad (5b)$$

where

$$J_0 = \frac{n^* \tau_{EM}}{4\tau_{FE}^2} \left(1 + \frac{1}{bn^* \tau_{EM}}\right) .$$

For this system $n_{EM}^0 \sim (n_{FE}^0)^2$ regardless of the recombination times. At low densities the excitons are dominant and $n_{FE}^0 \sim J$, while at high densities the molecules are dominant and $n_{EM}^0 \sim J$. If the molecular breakup rate bn^* is much greater than the recombination rate τ_{EM}^{-1}, the local form of the chemical equilibrium, $(n_{FE}^0)^2/n_{EM}^0 = n^*$, is obtained. If the recombination rate becomes comparable to the breakup rate, a deviation from the Arrhenius form of thermal activation occurs.[19] The absence of such deviations in the plots of R^* in Fig. 6 supports the idea of fast thermalization of EM and FE.

We may also test this hypothesis by exmaining the transient behavior of the EM-FE system. In the low-density, exciton-dominant regime the transient solution of Eqs. (5) is

$$n_{FE}(t) = n_{FE}^0 e^{-t/\tau_{FE}} \quad (6a)$$

and

$$n_{EM}(t) = n_{EM}^0 \left(e^{-t/\tau_1} - \frac{\tau_2}{\tau_1} e^{-t/\tau_2}\right) \Big/ \left(1 - \frac{\tau_2}{\tau_1}\right) , \quad (6b)$$

where

$$\frac{1}{\tau_1} = \frac{2}{\tau_{FE}} \quad \text{and} \quad \frac{1}{\tau_2} = \frac{1}{\tau_{EM}} + bn^* .$$

If intersystem thermalization is fast, $\tau_2 \ll \tau_1$, and

the second exponential in Eq. (6b) may be neglected giving

$$n_{EM}(t) \approx n^0_{EM} e^{-2t/\tau_{FE}} . \quad (6c)$$

In this case of quasiequilibrium, the apparent decay rate of the EM is predicted to be 2× faster than that of the FE. If the lifetimes become comparable to the thermalization time, the EM decay would exhibit a notable initial deviation from the exponential decay (6c) with duration of order τ_2.

To measure time decays a digital interval timer was developed which clocks the time between the laser turnoff and an emitted recombination photon, which was detected by a Varian *VPM*-164 photomultiplier. The measurements were accomplished under the very low-excitation levels of the previous thermodynamic measurements. At these levels the probability of one or more photons being detected per decay was less than 10%. The experiment was repeated at 10 kHz and a histogram of the time intervals was collected in a signal averager. Luminescence intensity decays over several orders of magnitude were easily obtainable with 1-meV spectral resolution and 100-ns time resolution. By focussing a YAlG:Nd laser precisely on the strain well, *e-h* pairs were created directly in the well, eliminating the transit times associated with surface excitation and increasing the production efficiency. The decay times were found to be independent of excitation level over wide limits. Time decays reported here proceed from the steady-state initial conditions with the laser ontime at least 5× the measured FE decay time constant.

The time decays for both EM and FE at $T = 5.2$ K are shown in Fig. 7. Both decays are exponential with lifetimes exceeding 2 μs, and the apparent lifetime ratio is 1.8, close to the predicted value of 2. The 10% discrepancy, reminiscent of the slight spatial discrepancy (Fig. 3), may indicate the degree to which the EM-FE systems achieves equilibrium. A temperature dependence of the time decays revealed a significant feature: the lifetimes are strongly temperature dependent with τ_{FE} increasing from 1.5 μs at 2 K to nearly 100 μs at 15 K. The increased lifetime at higher temperature may be caused by the reduced time an exciton spends on an impurity trap, due to evaporation.[14] However, the ratio of EM to FE decay rates is not sensitive to temperature nor does it change over a wide range of low level excitation.

These results are in agreement with the conclusions drawn from the steady-state data that intersystem thermalization occurs quite rapidly in comparison to recombination times.

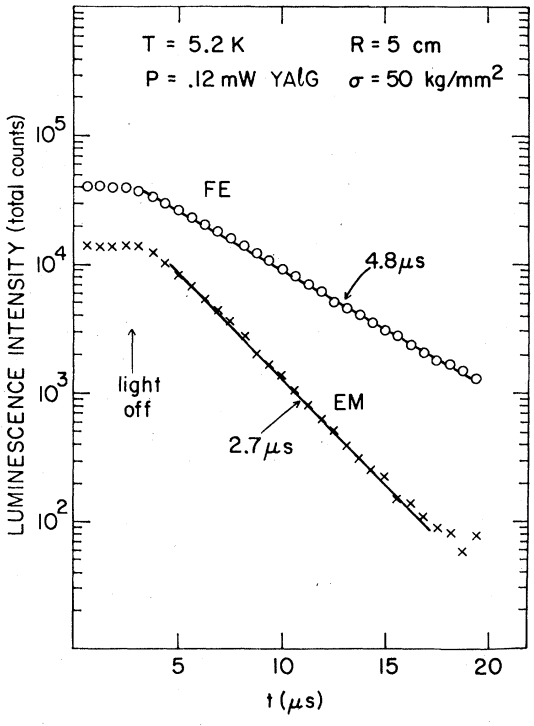

FIG. 7. Exponential time decays of the EM and FE luminescence peaks at $T = 5.2$ K showing that the ratio of the observed lifetimes is 1.8, close to the value of 2 predicted for quasiequilibrium.

VI. UNIFORM STRAIN

In addition to the spectroscopic measurements for the potential well, we have determined ϕ^s_{EM} for the TO-LO replica in uniformly stressed Si. This provides a check for the assumptions regarding the densities of states and allows a more direct comparison with the results of other workers. Figure 8 shows the line shape and fit (open points) for uniformly

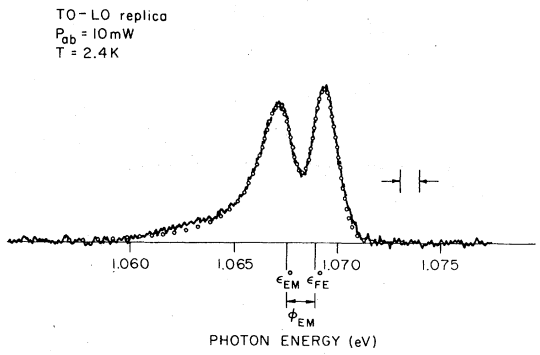

FIG. 8. Uniform stress spectrum and fit (open points) with all $D(\epsilon) \sim \epsilon^{1/2}$. The measured spectroscopic binding energy of this fit is 1.42 meV, very close to the average value obtained for the potential well, 1.46 meV. The $1 \times 1 \times 10$ mm^3 crystal is stressed uniaxially along a ⟨100⟩ axis and cw excited with an Ar^+ laser.

stressed Si. A comparison of the EM to FE peak height ratios of Figs. 8 and 5 along with the given temperatures and excitation levels indicates that the gas in the potential well occupies a much smaller volume. Thus the potential well provides a very effective means of producing a high density of excitons. The fitting procedure for the uniform stress case is identical with that described in the Appendix except that all $D(\epsilon) \sim \epsilon^{1/2}$. The results are displayed in Table I and show good agreement between ϕ_{EM}^{s} and ϵ_0 in the two stressing geometries. The value of σ_G is significantly larger in the uniform stress data. This is probably due to the sensitivity of the FE line to stress gradients because of its narrow linewidth at low temperatures and a wider spatial distribution for FE relative to that for EM.

In comparing the uniform stress line shape with that reported by Kulakovskii *et al.*,[4,5] there is good agreement for the peak separation and the shape of the EM low-energy tail. However, their data shows a 30% wider EM linewidth due to a broadening at the high-energy side. The reason for this broadening which influences the determination of ϕ_{EM}^{s} is not apparent.

Thewalt and Rostworowski[7] have determined $\phi_{EM}^{s} = 1.2$ meV for unstressed Si by fitting the TA replica with Cho's line shape. Their smaller value of ϕ_{EM}^{s} may be partly due to the mass-anisotropy splitting (0.31 meV) present in unstressed Si, which they did not consider explicitly. It is also possible that the molecular binding energy is slightly stress dependent, due to modification of the energy bands.

With high stress a fundamental simplification of the valence bands occurs which facilitates theoretical calculations of the binding energy and the analysis of the luminescence line shapes. Stress removes the conduction- and valence-band degeneracy and eliminates complications arising from small ground-state splittings of *e-h* complexes. In unstressed Si the FE ground state is split by 0.31 meV due to the conduction-band anisotropy.[20,21] For high enough stress the "upper" valence band is parabolic. The criterion for the "high-stress" limit" in the case of Boltzmann statistics is that kT be much less than the energy splitting of the light and heavy hole bands.[22] This criterion is satisfied by the stresses and temperatures used in this work.

VII. CONCLUSION

The measured binding energy $\phi_{EM} = 0.10 E_x$, with $E_x = 14.7$ meV the excitonic Rydberg, is considerably larger than the most recent calculations. Brinkman, Rice, and Bell,[23] Akimoto and Hanamura,[24] and most recently, Forney and Baldereschi[25] have calculated $\phi_{EM} = 0.03\ E_x$. Huang[26] found a larger value of 0.11 E_x. The results of Brinkman, Rice, and Bell suggest that the change in EM binding energy with stress is negligible since the electron to hole mass ratio is nearly identical in both the zero- and high-stress limits of Si. It should be noted, however, that the *total* calculated binding energy

$$E_{EM} = 2E_x^0 + 0.03E_x^0 = 2.03(12.8) = 26.1 \text{ meV}$$

differs by only 15% from the measured value

$$E_{EM} = 2E_{FE} + \phi_{EM} = 2(14.7) + 1.5 = 30.9 \text{ meV}$$

for the four-particle complex. E_x^0 is the isotropic FE Rydberg. The effect of anisotropy or exchange on molecule binding has not been calculated in detail for Si or Ge and may account in part for the discrepancy between theory and experiment.

The results of this investigation have provided clear thermodynamic evidence for the existence of the EM and have shown agreement between the thermodynamic and spectroscopic measurements of the binding energy. We have demonstrated the existence of a thermodynamic equilibrium between free excitons and excitonic molecules confined in a strain potential well in Si, shown the importance of thermal expansion of the excitonic gas in the determination of ϕ_{EM}^{t}, and presented evidence for rapid EM-FE thermalization within the particle lifetimes.

ACKNOWLEDGMENTS

We thank D. Guidotti and M. V. Klein for experimental assistance in obtaining the TA replica data and E. E. Haller for providing us with the Si sample. We also thank Greg Northrup and Mike Tamor for developing and constructing the interval timer. We acknowledge a Cottrell equipment grant by the Research Corporation which made the time-decay measurements possible. This work was supported by the National Science Foundation under the Materials Research Laboratory Grant No. DMR-77-23999.

APPENDIX: PROCEDURE FOR FITTING THE EM-FE SPECTRA

To fit the experimental spectra, we superposed Cho's EM line shape[12] with a Gaussian-broadened FE line. The superposition with coefficients A and B is

$$I'(h\nu') = AI_{EM}(h\nu' - \epsilon_{EM}^0) + BI_{FE}(h\nu' - \epsilon_{FE}^0) \ . \quad (7)$$

I_{EM} and I_{FE} are the component line shapes normalized to unit height and given explicitly by

$$I_{EM}(h\nu';\epsilon_0,r_m,T) = I_{EM}^0 \int d\epsilon\, D_{EM}^{L}(\epsilon) e^{-\epsilon/kT} D_{FE}^{F}(\epsilon - h\nu') \times (\{\tfrac{3}{2}\epsilon - h\nu' - [r_m\epsilon(\epsilon - h\nu')]^{1/2} + \epsilon_0\}^{-3} - \{\tfrac{3}{2}\epsilon - h\nu' + [r_m\epsilon(\epsilon - h\nu')]^{1/2} + \epsilon_0\}^{-3}) \quad (8)$$

and

$$I_{\mathrm{FE}}(h\nu';\sigma_G,T) = I^0_{\mathrm{FE}} \int d\epsilon\, D^I_{\mathrm{FE}}(\epsilon)\, e^{-\epsilon/kT} e^{-(h\nu'-\epsilon)^2/2\sigma_G^2} . \quad (9)$$

The I_i^0 are normalization factors, $r_m = m_{\mathrm{EM}}/m_{\mathrm{FE}}$ is the ratio of translational masses, $\epsilon_0 = \hbar^2/2ma^2_{\mathrm{EM}}$ is a broadening parameter in energy units, and a_{EM} defines the spatial extent of the EM wave function. The parameter σ_G is the standard deviation of the Gaussian-broadening function. The final density of states, D^F_{FE}, accessible to the FE remaining after the radiative EM decay is that for a free particle, $\sim\epsilon^{1/2}$, since the EM decay occurs locally in space.

The initial densities of states, D^I_{EM} and D^I_{FE}, are determined from the following arguments. For a spatially dependent single-particle energy of the form $E_i = E_i(\vec{k},\vec{r})$ the corresponding density of states is

$$D_i(\epsilon) = \frac{g_i}{(2\pi)^3} \int d^3k \int d^3r\, \delta(\epsilon - E_i(\vec{k},\vec{r})) . \quad (10)$$

We assume that

$$E_i(\vec{k},\vec{r}) = \frac{h^2k^2}{2m_i} + \alpha_i r^2 . \quad (11)$$

The basis for the parabolic momentum dispersion rests on the arguments given previously for the high-stress limit and on theoretical calculations finding parabolic exciton dispersion in the more complicated case (degenerate valence bands) of unstressed Si.[20] Although similar calculations for the more complicated EM are currently unavailable, we expect the ground state to lie deep enough to exhibit parabolic dispersion.[20] The harmonic approximation to the spatial potential is justified by the Gaussian spatial profiles of Fig. 3.

Evaluating (10) with the given single-particle energy (11) we find

$$D_i(\epsilon) = \tfrac{1}{16} g_i \left(\frac{2m_i}{\hbar^2\alpha_i}\right)^{3/2} \epsilon^2 . \quad (12)$$

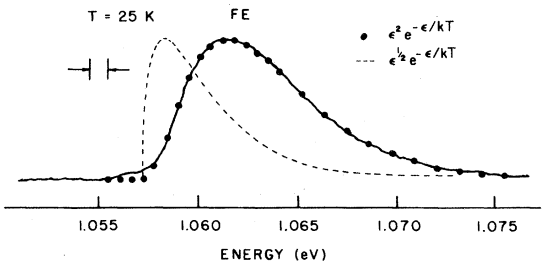

FIG. 9. High-temperature FE line shape showing the excellent fit of the simple fitting function with $D(\epsilon) \sim \epsilon^2$. For comparison, the usual FE fitting function with $D(\epsilon) \sim \epsilon^{1/2}$ is shown (broken line).

The same result is obtained from a simple quantum-mechanical consideration of the 3-D harmonic oscillator.[6] Thus the effect of a parabolic strain potential is to replace the usual density of states $D(\epsilon) \sim \epsilon^{1/2}$ with $D(\epsilon) \sim \epsilon^2$. Above $T \approx 6$ K, the Gaussian-broadening parameter σ_G of Eq. (9) makes a negligible contribution to the FE linewidth, obviating the broadening intergral so that

$$I_{\mathrm{FE}}(h\nu) = I^0_{\mathrm{FE}}(h\nu - \epsilon^0_{\mathrm{FE}})^2 \times \exp[-(h\nu - \epsilon^0_{\mathrm{FE}})/kT] . \quad (13)$$

The remarkable agreement between this simple fitting function and the FE line shape is shown in Fig. 9. This data in addition to that of Fig. 5 for $T > 6$ K firmly support the ϵ^2 density of states.

The mass ratio was fixed at $r_m = 2$. This choice seems reasonable in view of the good agreement between calculated exciton translational masses in Si (Ref. 20) and the result obtained from simple classical consideration. In all fits the temperature was set equal to the measured lattice temperature.

The final form of the fitting function was obtained after convolving the superposition, Eq. (7), with the measured slit function $S(\epsilon)$

$$I(h\nu'') = \int d(h\nu') S(h\nu' - h\nu'') I'(h\nu') . \quad (14)$$

Since the fitting function was normalized to the FE peak, only the relative height $\rho \equiv A/B$ was adjusted. For convenience, two fitting parameters were redefined: the molecule binding energy $\phi_{\mathrm{EM}} \equiv \epsilon^0_{\mathrm{FE}} - \epsilon^0_{\mathrm{EM}}$ and $h\nu_s \equiv \epsilon^0_{\mathrm{EM}} - \epsilon_{\mathrm{ref}}$, the energy shift of the EM zero position with respect to an energy reference, ϵ_{ref}, for the experimental spectrum.

Thus the final form of the composite fitting function involved five adjustable parameters

$$I = I(h\nu'';\epsilon_0, \sigma_G, \rho, \phi_{\mathrm{EM}}, h\nu_s) . \quad (15)$$

All five fitting parameters were varied in a least-squares-fitting procedure to determine spectroscopic parameters ϵ_0, σ_G, and ϕ_{EM} for spectra recorded at different temperature, excitation level, stress, and for both TA and TO-LO replicas. These results are summarized in Table I.

The fitting parameters ϵ_0, σ_G, and ϕ_{EM} did not vary appreciably with temperature. This permitted the relative numbers of EM and FE to be accurately determined as a function of temperature by fitting spectra at each temperature, adjusting only the relative height ρ and fixing the other parameters at their average values. The relative numbers were calculated by numerical integration of the isolated line shapes.

[1]M. A. Lampert, Phys. Rev. Lett. 1, 450 (1958).
[2]See the review by E. Hanamura and H. Haug, Phys. Rep. 33, 1 (1977).
[3]I. Pelant, A. Mysyrowicz, and C. Benoit á la Guillaume, Phys. Rev. Lett. 37, 1708 (1976).
[4]V. D. Kulakovskii and V. B. Timofeev, JETP Lett. 25, 458 (1977).
[5]V. D. Kulakovskii, V. B. Timofeev, and V. M. Edelstein, Zh. Eksp. Teor. Fiz. 74, 372 (1978); in *Proceedings of the 14th International Conference on the Physics of Semiconductors, Edinburgh, 1978,* edited by B. L. H. Wilson (Institute of Physics and Physical Society, London, 1979).
[6]P. L. Gourley and J. P. Wolfe, Phys. Rev. Lett. 40, 526 (1978).
[7]M. L. W. Thewalt and J. A. Rostworowski, Solid State Commun. 25, 991 (1978).
[8]G. A. Thomas and T. M. Rice, Solid State Commun. 23, 359 (1977).
[9]R. S. Markiewicz, J. P. Wolfe, and C. D. Jeffries, Phys. Rev. B 15, 1988 (1977).
[10]J. P. Wolfe, R. S. Markiewicz, S. M. Kelso, J. E. Furneaux, and C. D. Jeffries, Phys. Rev. B 18, 1479 (1978).
[11]A more detailed description of the spatial distribution must include the anisotropy of the deformation potential and the stress distribution, but we expect the form of the temperature dependence to remain unaltered.
[12]K. Cho, Opt. Commun. 8, 412 (1973).
[13]V. D. Kulakovskii and V. B. Timofeev, in *Proceedings of the 14th International Conference on the Physics of Semiconductors, Edinburgh, 1978,* edited by B. L. H. Wilson (Institute of Physics and Physical Society, London, 1979).
[14]R. B. Hammond and R. N. Silver (unpublished).
[15]C. Benoit á la Guillaume, F. Salvan, and M. Voos, in *Proceedings of the International Conference on Luminescence, Newark, 1969* (North-Holland, Amsterdam, 1970), p. 315.
[16]L. V. Keldysh, in *Eksitony v Poluprovodnikakh* (Nauka, Moscow, 1971).
[17]V. M. Asnin, V. V. Zubor, T. M. Marina, A. M. Prokhorov, A. A. Rogachev, and N. I. Sablina, Sov. Phys. JETP 35, 390 (1972).
[18]B. V. Zubov, V. P. Kalinushkin, T. M. Marina, A. M. Prokhorov, and A. A. Rogachev, Sov. Phys. Semicond. 7, 1077 (1974).
[19]The deviation from Arrhenius thermal activation has been reported for a system of FE and bound multiexciton complexes in Si. See S. A. Lyon, D. L. Smith, and T. C. McGill, Phys. Rev. Lett. 41, 56 (1978).
[20]M. Altarelli and N. O. Lipari, Phys. Rev. B 15, 4898 (1977).
[21]R. B. Hammond and R. N. Silver, Solid State Commun. 28, 993 (1978).
[22]G. L. Bir and G. E. Pikus, *Symmetry and Strain-Induced Effects in Semiconductors* (Keter Publishing, Jerusalem, 1974).
[23]W. F. Brinkman, T. M. Rice, and B. Bell, Phys. Rev. B 8, 1570 (1973).
[24]O. Akimoto and E. Hanamura, J. Phys. Soc. Jpn. 33, 1537 (1972).
[25]J. J. Forney and A. Baldereschi, in *Proceedings of the 14th International Conference on the Physics of Semiconductors, Edinburgh, 1978,* edited by B. L. H. Wilson (Institute of Physics and Physical Society, London, 1979).
[26]W. T. Huang, Phys. Status Solidi B 60, 309 (1973).

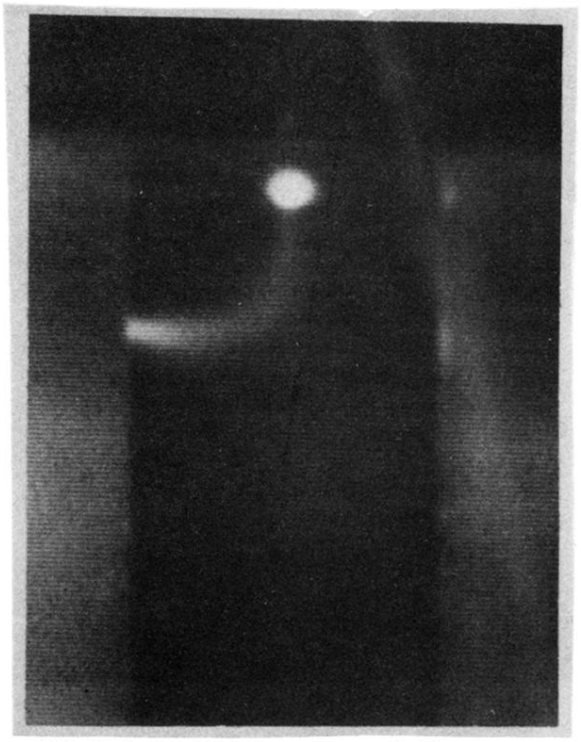

FIG. 2. Exciton luminescence emanating from a $1.5 \times 1.5 \times 4$ mm^3 crystal of ultrapure Si at $T \approx 10$ K. The top crystal surface, accurately flattened and polished, is pressed with a spherical contacting surface of a steel plunger cut from a ball bearing with radius $R = 3.8$ cm. Excitons produced at the left crystal surface by a cw Ar laser are drawn into a parabolic potential well corresponding to a shear strain maximum beneath the plunger.